Evolution of magnetism, valence, and crystal lattice in EuCd$_2$As$_2$ under pressure

Greeshma C. Jose [1], Kaleb Burrage,[1] Jose L. Gonzalez Jimenez [2], Weiwei Xie,[2] Barbara Lavina [3,4], Jiyong Zhao,[4] Esen E. Alp,[4] Dongzhou Zhang,[5] Yuming Xiao,[6] Yogesh K. Vohra,[1] and Wenli Bi [1,*]

[1]*Department of Physics, University of Alabama at Birmingham, Birmingham, Alabama 35294, USA*
[2]*Department of Chemistry, Michigan State University, East Lansing, Michigan 48824, USA*
[3]*Center for Advanced Radiation Sources, The University of Chicago, Chicago, Illinois 60637, USA*
[4]*Advanced Photon Source, Argonne National Laboratory, Argonne, Illinois 60439, USA*
[5]*Hawaii Institute of Geophysics and Planetology, School of Ocean and Earth Science and Technology,*
University of Hawaii at Manoa, Honolulu, Hawaii 96822, USA
[6]*HPCAT, X-ray Science Division, Argonne National Laboratory, Argonne, Illinois 60439, USA*

EuCd$_2$As$_2$ has been proposed to be one of the ideal platforms as an intrinsic topological magnetic system, potentially hosting a single pair of Weyl points when it is tuned into the ferromagnetic state with spins aligned out of plane by either external pressure or chemical doping. To investigate the possible realization of an ideal topological state, we have systematically investigated pressure control of the magnetic state, valence, and crystal structure using synchrotron-based time-domain Mössbauer spectroscopy, x-ray absorption spectroscopy, and powder x-ray diffraction. Our experimental results show that the magnetic configuration remains mostly in plane under pressure up to 42.8 GPa and pressure effectively enhances the magnetic ordering temperature. Meanwhile, Eu ions remain divalent when subjected to pressure up to 35.9 GPa, and the trigonal crystal lattice is maintained up to 34.6 GPa. Our work provides valuable experimental data to benchmark future theoretical studies in magnetic topological materials.

I. INTRODUCTION

Topological materials have attracted significant interest in condensed matter research due to their macroscopic quantum phenomena with the potential as excellent candidates for technological applications in spintronics, magnetoelectronics, and quantum computing [1–6]. In particular, Dirac and Weyl semimetals are narrow gap materials where the conduction band and valence bands touch linearly at discrete nodal points in the momentum space. The low-energy excitation near the nodal points disperses linearly and can be described by the massless relativistic Dirac/Weyl equation [7,8]. When either time-reversal symmetry or spatial inversion symmetry, or both, is broken, the Dirac point splits into a pair of Weyl points of opposite chirality. Magnetic Weyl semimetals with time-reversal breaking are a recently discovered class of materials that show novel transport properties such as negative magnetoresistance, chiral magnetic effect, and anomalous Hall effect [2,5,8–13].

In the search for magnetic Weyl semimetals, EuCd$_2$As$_2$ was proposed to be a suitable candidate as it can host multiple topological phases in different magnetic configurations [14–17]. It has been shown that EuCd$_2$As$_2$ can be a topological insulator in the antiferromagnetic (AFM) phase with Eu moments lying in the *ab* plane [14,15,18–20] and a potentially ideal Weyl semimetal when it is in the ferromagnetic (FM) phase with the moments aligned along the *c* axis. EuCd$_2$As$_2$ crystallizes in a layered centrosymmetric trigonal lattice structure with the $P\bar{3}m1$ space group [21]. While the conduction electrons are contributed by tetrahedra Cd-As layers, the long-range magnetic order is due to the triangular Eu^{2+} ($4f^7$) sublattices [21–23]. Previous reports reveal that Eu $4f$ moments order below 9.5 K with a type-A AFM structure where FM *ab* planes stack antiferromagnetically along the *c* axis [18,22–24]. Several methods have been suggested and experimented with to introduce and stabilize the Weyl semimetal phase in EuCd$_2$As$_2$, including application of external magnetic field, pressure, and chemical doping [15,16,19,25–27].

Earlier studies up to 2.5 GPa using high-pressure muon spin spectroscopy have reported an in-plane antiferromagnetic (AFM$_{ab}$) to in-plane ferromagnetic (FM$_{ab}$) transition at 2 GPa and have predicted a further transition to an out-of-plane ferromagnetic state (FM$_c$) around 23 GPa, provided that Eu remains in a divalent state [25]. For Eu ions, the divalent state has total angular momentum $J = 7/2$, while the trivalent state ($4f^6$) is nonmagnetic ($J = 0$). Since the valence state of Eu is closely related to the magnetic state, and the valence transition in Eu-based systems is commonly discussed, a simultaneous study of valency is needed to provide insights into a possible change in magnetic order.

Following these findings, there is a need to extend the study in EuCd$_2$As$_2$ to higher pressures in order to provide information on the proposed pressure-induced Weyl state. In this work, we report a systematic investigation of the magnetism,

*Corresponding author: wbi@uab.edu

Eu valence state, and crystal structure using time-domain synchrotron Mössbauer spectroscopy (SMS), x-ray absorption spectroscopy (XAS), and powder x-ray diffraction (XRD) up to 42.8, 35.9, and 34.6 GPa, respectively. Our high-pressure study establishes that the magnetic moments in $EuCd_2As_2$ remain mostly in plane, while the magnetic ordering temperature (T_o) is enhanced monotonically with pressure. The Eu divalent state as well as trigonal crystal lattice are stable in the measured pressure range.

II. EXPERIMENTAL METHODS

Starting elements (Eu pieces, 99%; Cd drops, 99.99%; As lumps, 99.9%; Sn drops, 99.999%, all from Alfa Aesar) were mixed with an atomic ratio of Eu:Cd:As:Sn = 1:2:2:20 inside the Al_2O_3 crucible, which was then sealed inside a quartz tube along with quartz wool and glass pieces used to filter the flux. The tubes were heated to 900 °C at 30 °C/h and held for 24 hours. Then the tubes were slowly cooled to 750 °C at a rate of 3 °C/h and held for 50 hours. The product was centrifuged to remove the Sn flux. The silver color crystals are stable in the air.

Mössbauer spectroscopy is a well-established technique to study magnetic and valence transitions in materials with suitable isotopes such as ^{151}Eu (natural abundance 47.8%, half life 9.7 ns). The magnetic state of $EuCd_2As_2$ was investigated using time-domain SMS. Benefiting from the focused beam and brilliant x rays, SMS has been widely applied in high-pressure magnetic studies [28–32]. The experiments were conducted at the Beam line 3ID of the Advanced Photon Source (APS), Argonne National Laboratory (ANL), at the nuclear resonant energy of ^{151}Eu (21.54 keV). The measurements were performed during a 24-bunch timing mode with 153 ns between consecutive electron bunches for Mössbauer data collection in time domain. To reach high pressure and low temperature, a miniature diamond anvil cell (DAC) and a compatible helium flow cryostat were used [33]. High pressure up to 42.8 GPa was achieved using a pair of diamond anvils with 300-μm-diameter culet size. A rhenium (Re) gasket was preindented to 50 μm thickness and a hole of 150 μm diameter was electrosparked to serve as the sample chamber. A single-crystal sample was loaded in the sample chamber with the crystallographic *c* axis along the direction of the incident x rays. The sample orientation was closely monitored during the pressure application and cooling/warming cycle using an online microscope and no visible change was observed. Ruby balls were loaded in the sample chamber as an *in situ* pressure marker. Pressures were determined from the shift of the *R*1 line of ruby fluorescence [34]. Neon gas was used as the quasihydrostatic pressure-transmitting medium at high-pressure and low-temperature conditions. Other than the initial pressure which was applied at room temperature after neon gas loading, all subsequent pressures were applied at 100 K through a helium gas membrane. The CONUSS program [35] was used to evaluate the SMS data and extract hyperfine parameters such as the magnetic hyperfine field (B_{hf}) and electric quadrupole interaction (Δ). To obtain information on the valence state of Eu ions, the isomer shift (δ) of ^{151}Eu was measured using a trivalent Eu_2O_3 (δ: 1.024 mm/s relative to EuF_3) as a reference sample [36,37].
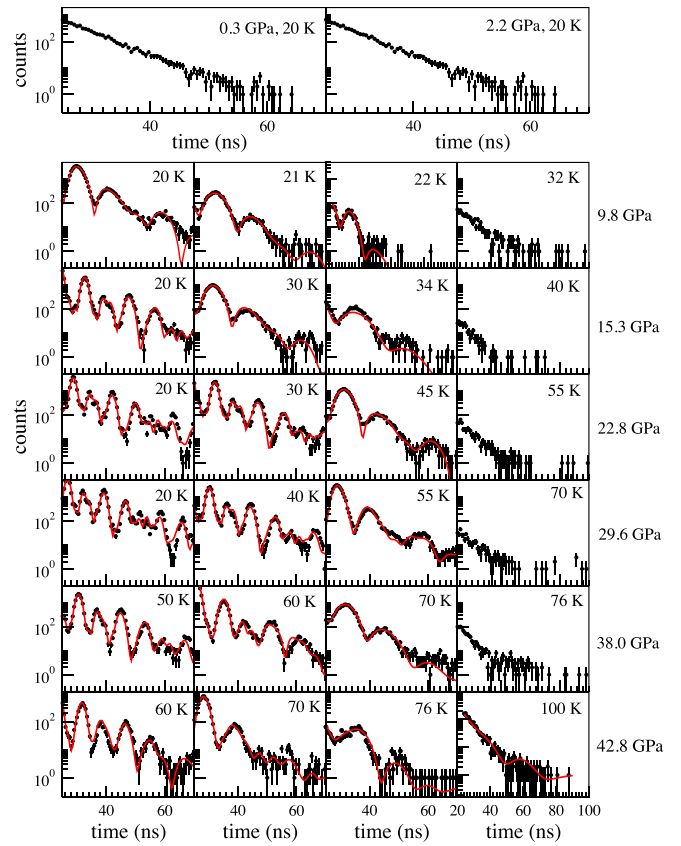

FIG. 1. SMS spectra of ^{151}Eu in $EuCd_2As_2$. The black dots represent the experimental data and the red lines correspond to fits from the CONUSS program.

To directly probe the valence state of Eu, partial fluorescence yield–x-ray absorption spectroscopy (PFY-XAS) at Eu's L_3 edge (6.977 keV) was conducted at the 16ID-D beam line of the APS, ANL [38]. The x-ray beam was focused to 4.6×6 μm (FWHM). The measurements were carried out at room temperature using a pair of diamond anvils with 300 μm culet size to generate pressure up to 37 GPa. X-ray energy was scanned from 6.957 to 7.027 keV with a 0.5 eV step. Due to strong absorption by diamond anvil in this energy range, the experiment was performed with incident x rays perpendicular to the loading axis in the diamond anvil cell and traveling through the beryllium (Be) gasket. In order to preserve the sample thickness under compression, cubic boron nitride and an epoxy mixture were used as an insert. A 110 μm hole was manually created at the center of the gasket insert as the sample chamber. Pressures were determined from ruby fluorescence [34]. To avoid self-absorption, the sample position was optimized by carefully scanning the sample. The L_{α_1} emission line (5.845 keV) was selected with the silicon analyzer located perpendicular to the incident x-ray beam. The signal was then collected by a Pilatus 100 K detector. The data were normalized by the difference of pre-edge and post-edge absorption using ATHENA software [39] to account for any variation of sample thickness throughout the experiment.

To inspect the crystal structure at high pressures, a room-temperature angle-dispersive XRD experiment was conducted

TABLE I. List of B_{hf}, angle (θ) between B_{hf} and x-ray propagation direction, quadrupole interaction (Δ), and isomer shift (δ) of ^{151}Eu in EuCd$_2$As$_2$ at high pressures (P) and various temperatures (T). Uncertainties generated from data fitting in CONUSS are shown in parentheses.

P (GPa)	T (K)	B_{hf} (T)	θ (deg)	Δ (mm/s)	δ (mm/s)
0.3	20	0			
2.2	20	0			
	20	20.24(4)	74(1)	3.7(2)	
	21	18.59(7)	57.4(8)	3.7(1)	
9.8	22	17.1(1)	55(2)	3.7(2)	
	23	16.5(1)	61(3)	3.7(1)	
	32	0			
	100	0		2.47(3)	−10.16(2)
	20	25.49(2)	82.2(6)	4.1(1)	
	25	21.54(1)	104(1)	4.1(1)	
15.3	30	19.30(3)	136.9(8)	4.01(7)	
	32	17.98(4)	126.3(7)	3.9(2)	
	34	10.85(3)	91(1)	3.9(5)	
	36	3.19(5)	122.0(5)	3.73(4)	
	40	0			
	100	0		2.74(4)	−9.68(3)
	20	29.12(3)	77(2)	5.1(1)	
	25	27.16(3)	88(2)	4.7(1)	
	30	25.93(3)	87.1(9)	4.4(1)	
22.8	35	24.52(3)	84(1)	3.9(1)	
	45	19.15(2)	59(3)	2.1(2)	
	50	9.60(5)	120(1)	0.8(1)	
	55	0			
	100	0		2.55(3)	−8.82(2)
	20	31.16(3)	81.7(7)	5.2(1)	
	30	29.20(3)	89(1)	4.8(1)	
	40	27.49(3)	85(3)	4.6(1)	
29.6	50	23.48(4)	91(3)	4.7(1)	
	55	20.90(2)	119(2)	4.7(1)	
	65	15.35(3)	145(3)	4.9(1)	
	70	0			
	100	0		2.80(3)	−8.28(2)
	40	29.80(2)	76.6(7)	4.6(1)	
	50	27.18(2)	90(1)	4.7(1)	
38.0	60	23.62(3)	90(1)	4.4(1)	
	70	18.51(2)	114.4(9)	4.41(5)	
	76	0			
	100	0		2.60(3)	−7.92(2)
	60	26.28(2)	77(1)	5.0(1)	
	70	21.47(3)	128(3)	5.01(7)	
42.8	76	12.5(2)	103(3)	4.6(3)	
	100	0		2.5(3)	
	110	0		2.5(4)	−7.72(2)

at the 13BM-C beam line (PX^2) of the APS, ANL [40] using x rays with a wavelength of 0.434 Å. To acquire pressures up to 35 GPa, a BX-90 DAC with Boehler-Almax anvils of 500 μm culet was used. A Re gasket which was intended to 82 μm and drilled with a 250 μm hole was placed between the anvil to create the sample chamber. A single-crystalline sample was ground into powder and loaded in the chamber along with ruby balls as an *in situ* pressure marker [34]. Neon was used
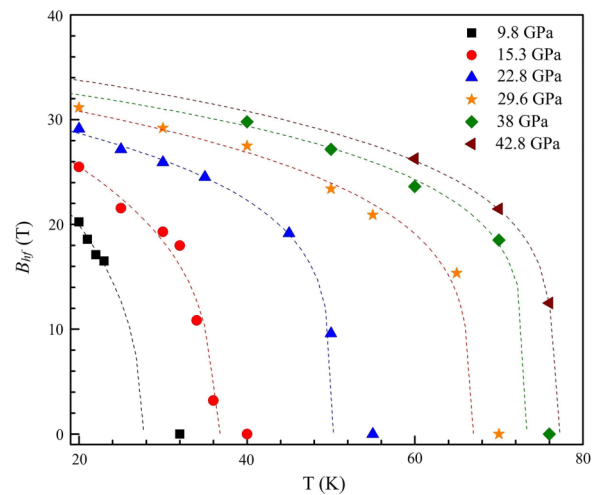

FIG. 2. Extracted magnetic hyperfine field of ^{151}Eu in EuCd$_2$As$_2$ as a function of temperature at various pressures. The dashed lines serve as a guide to the eye.

as a pressure-transmitting medium. The two-dimensional (2D) diffraction images were integrated using the DIOPTAS software [41]. LeBail refinements on the high-pressure XRD data were performed in GSAS-II [42].

III. RESULTS AND DISCUSSION

Earlier study showed that the magnetic ground state of EuCd$_2$As$_2$ can be controlled from AFM to FM by changing the growth methods [19]. It is reported that EuCd$_2$As$_2$ manifest AFM order below 9.5 K [25] using Sn flux. And EuCd$_2$As$_2$ can be tuned from AFM with T_N of 9.2 K to FM with T_C of 26.4 K using salt solution growth. Magnetization data taken on our sample confirm the AFM ground state (see the Appendix).
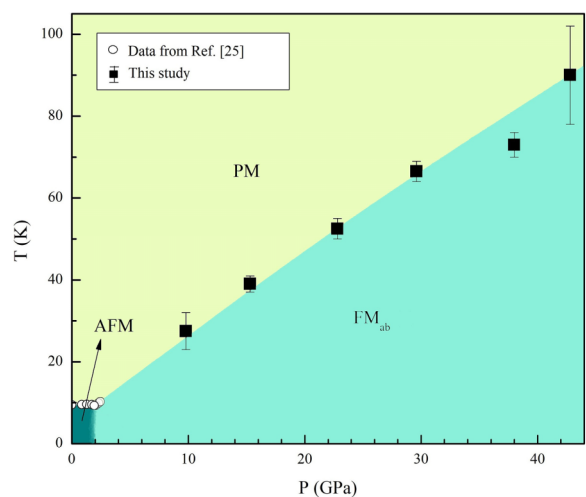

FIG. 3. The temperature-pressure phase diagram summarizes the SMS results combined with previous studies up to 2.5 GPa from Ref. [25]. Pressure drives EuCd$_2$As$_2$ from a type-A AFM state to an in-plane FM (FM$_{ab}$) state around 2 GPa. At higher pressure, the SMS data suggest that the magnetic moments remain in the *ab* plane (FM$_{ab}$) up to 42.8 GPa.
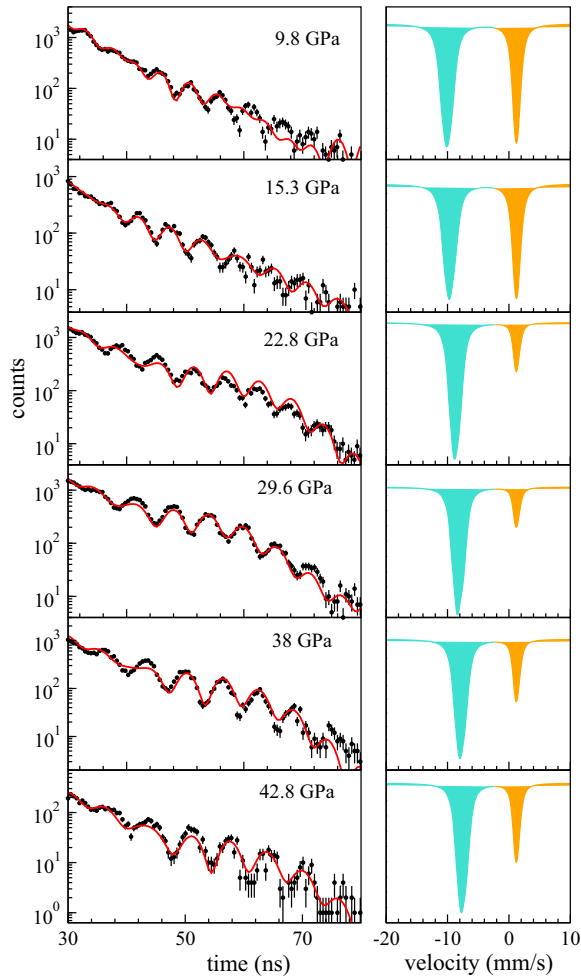
FIG. 4. ^{151}Eu SMS spectra for various pressures at 100 K in EuCd$_2$As$_2$ with Eu$_2$O$_3$ as reference which is located at ambient conditions. The simulated energy-domain spectra corresponding to each pressure are plotted in the right column, with shaded blue lines representing resonant absorption from EuCd$_2$As$_2$ and shaded orange lines representing absorption from the reference sample Eu$_2$O$_3$.

FIG. 5. PFY-XAS plot for the Eu L_3 edge in EuCd$_2$As$_2$ for different pressures, ranging from ambient pressure (AP) to 35.9 GPa, taken at room temperature.

The representative SMS spectra for EuCd$_2$As$_2$ at different temperatures and pressures are shown in Fig. 1. The experimental data were fitted using CONUSS software [35], which uses the time spectra of forward nuclear resonant scattering to derive hyperfine parameters. The two hyperfine parameters, i.e., magnetic hyperfine field and electric quadrupole interaction, along with the sample effective thickness were used as variables for fitting the data. For $4f^7$ ions, a magnetic hyperfine field arises due to contributions from core electron polarization, the polarization of conduction electrons by ion, and by neighboring atoms [28,43]. In the presence of magnetic order, due to the Zeeman splitting of nuclear levels, quantum oscillations emerge in the SMS spectrum [28]. Quadrupole interaction contributes to additional beating frequency. At constant pressure, the oscillation frequency decreases as the temperature is raised due to a decrease in B_{hf}. The oscillations disappear as the system enters the paramagnetic phase. It is evident from Fig. 1 that at 20 K, as pressure increases from 9.8 to 22.8 GPa, higher-frequency quantum beats evolve in the
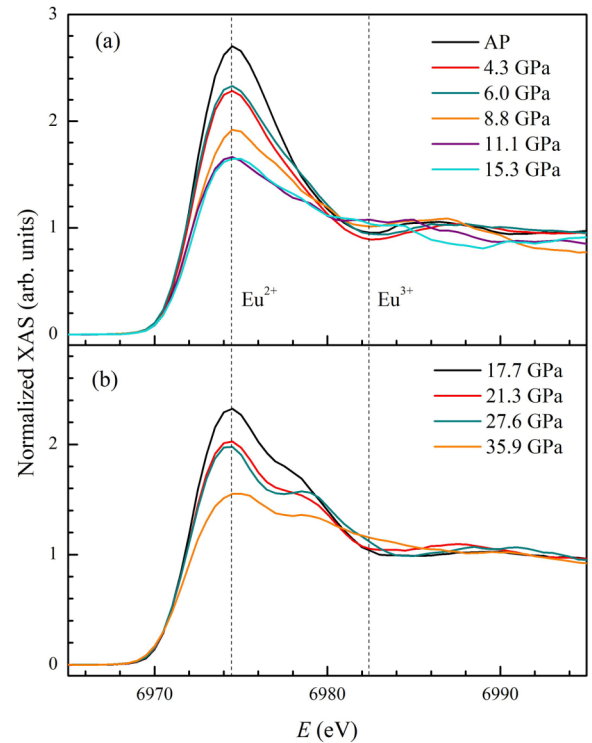
spectra, indicating increasing of B_{hf}. This can be attributed to the larger energy splitting in nuclear levels due to the B_{hf} of magnetically ordered states. As pressure is raised, T_o increases drastically, reaching a temperature above 76 K at 42.8 GPa.

Table I contains a list of parameters extracted from the fitting of curves using CONUSS. The B_{hf} values vs temperature are plotted in Fig. 2 for various pressures showing a monotonic increase of T_o. This increase is likely due to enhanced exchange interaction with reduced atomic distance [44]. Furthermore, the angle (θ in Table I) between the magnetic hyperfine field (B_{hf}) and the propagation direction of the linearly polarized x rays can be obtained from fitting the SMS data. This angle reflects the magnetic configuration. The analysis shows that B_{hf} remains mostly perpendicular to the x rays, indicating that magnetic moments lie in plane throughout this pressure range, contrary to the earlier prediction that a pressure of 23 GPa will stabilize the FM state along the c axis [25,44].

The values of quadruple interaction are also tabulated in Table I. The Δ mainly depends on the electric field gradient (EFG) at the nucleus caused by the charge distribution in the lattice and incompletely filled electronic shells. For Eu^{2+}, the $4f$ shell is half filled, making the electronic ground state isotropic ($^8S_{7/2}$) according to Hund's rule [45] and the zero total angular momentum gives no electronic contribution to Δ. Hence, the Δ values largely reflect the EFG from lattice contribution. The extracted electric quadruple interaction of 3.7 to 5.25 mm/s are typical values for Eu-based compounds.

Combining the results up to 2.5 GPa from Ref. [25], a temperature-pressure magnetic phase diagram of EuCd$_2$As$_2$
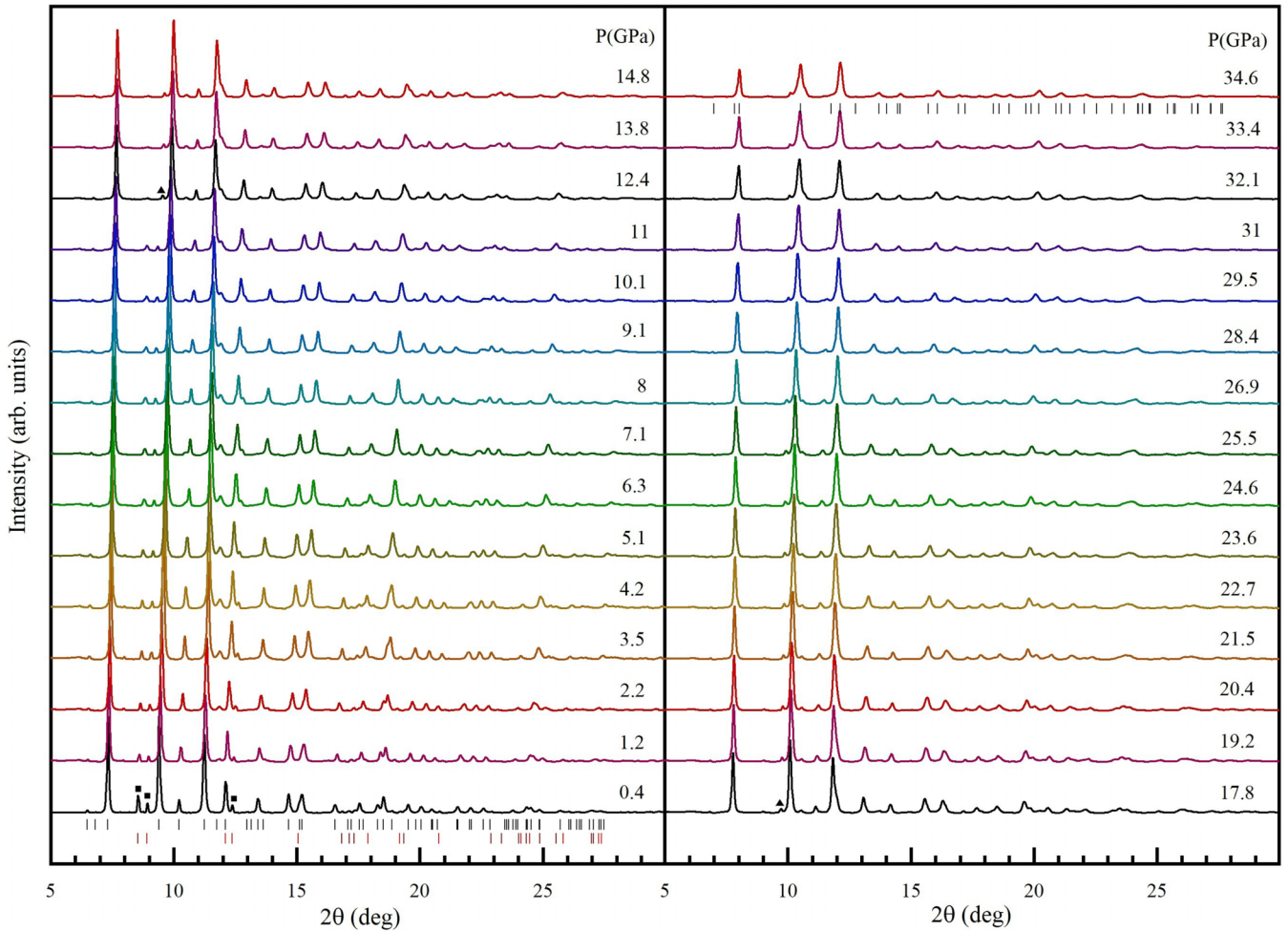
FIG. 6. XRD spectra of $EuCd_2As_2$ under pressure up to 34.6 GPa. In this pressure range, the Bragg peaks can be indexed with the $P\bar{3}m1$ space group. Black and red tick marks represent the peak positions for $EuCd_2As_2$ and a minor Sn impurity phase, respectively. The solid square and triangle symbols indicate β-Sn and γ-Sn phases below and above 11 GPa.

is constructed in Fig. 3. The value of T_o is estimated by taking the average of two temperature points between which the SMS spectra showed the transition from a magnetic to paramagnetic state. At each pressure, the error bars for T_o are estimated from the difference between the highest temperature measured at which $EuCd_2As_2$ displays nonzero B_{hf} and the lowest temperature where $EuCd_2As_2$ enters a paramagnetic state, shown in Fig. 2.

The large difference in the isomer shift values for the Eu^{2+} and Eu^{3+} valence states makes it useful to study a possible valence transition induced by pressure. To determine the δ values, SMS data were taken with Eu_2O_3 as a reference in the paramagnetic state at 100 K (Fig. 4). At 77 K and ambient pressure, δ of $EuCd_2As_2$ was reported to be -11.67 mm/s from conventional transmission Mössbauer spectroscopy [21]. Under pressure, δ increases to -10.16 mm/s at 9.8 GPa and then to -7.72 mm/s at 42.8 GPa (Table I). However, precautions should be taken to interpret the change in isomer shift. This change cannot be solely attributed to a valence change. Other mechanisms such as compression of 6s electrons and increase of exchange interactions involving the f, d, p, and s electrons can also lead to a significant change in the δ value [36]. The general tendency of the isomer shift value versus

pressure shows a continuous increase with the increase in pressure. To provide further information on the valence state of Eu ions, a PFY-XAS experiment was conducted.

The absorption edge energy of a specific element is sensitive to the oxidation state of the absorbing atom. In the case of the L_3 edge of Eu ($2p_{3/2} \rightarrow 5d$), the absorption peak shifts by 8 eV toward higher energy when the transition occurs from Eu^{2+} to Eu^{3+}. This large energy shift makes it convenient to detect a valence transition. It can be seen from the normalized XAS spectra (Fig. 5) that Eu remains divalent under pressure up to 35.9 GPa.

The absorption peak intensity, which heavily depends on the number of unoccupied states in the final d orbital, decreases under pressure. Interestingly, above 15.3 GPa, a double-peak structure in the absorption peak develops. It is noted that the new peak appears at an energy of 4 eV higher than the original one, which is a much lower energy than the absorption peak from the Eu^{3+} state, ruling out the possibility of a transition from divalent to trivalent state. The double-peak feature is likely caused by the splitting of d bands by the crystal field and population change of e_g and t_{2g} subsets of the d orbitals [46]. Based on the current information, it can be safely concluded that the increase of δ does
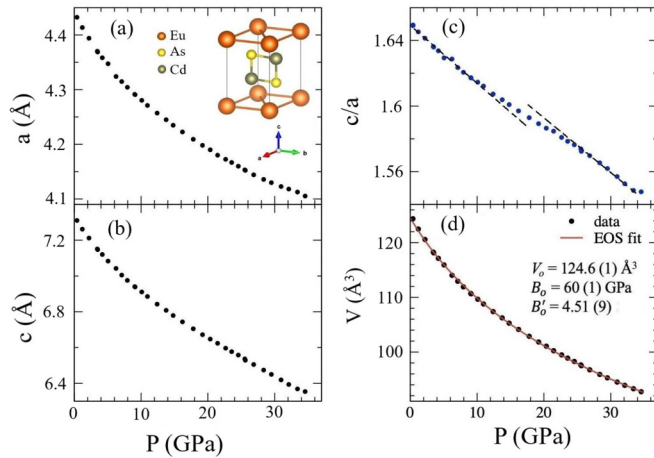
FIG. 7. Lattice parameters and volume in $EuCd_2As_2$ under pressure. The inset shows the crystal structure of $EuCd_2As_2$ in one unit cell. The Eu, Cd, and As atoms are represented by orange, green, and yellow solid circles, respectively.
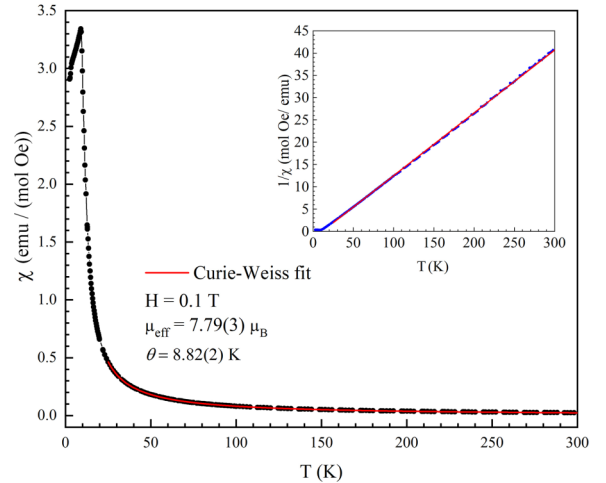

FIG. 8. Magnetic susceptibility data with zero-field cooling and Curie-Weiss fitting for the data in the 25–300 K region. The plot of $1/\chi$ is shown in the inset.

not signal a $4f^7$ to $4f^6$ transition. The crystal structure of $EuCd_2As_2$ was investigated under pressures up to 34.6 GPa using synchrotron powder XRD. As shown in Fig. 6, the Bragg peaks shift toward the higher angles as pressure is increased. The XRD data can be indexed with the trigonal structure (P$\bar{3}m1$), indicating that the ambient centrosymmetric trigonal structure is stable up to 34.6 GPa. A minor β-Sn impurity phase was observed in the XRD data at 0.4 GPa and included in the analysis. Since β-Sn ($I4_1amd$) undergoes a phase transition to γ-Sn ($I4/mmm$) around 10 GPa [47,48], the γ-Sn phase was included for the analysis above 10 GPa. Figure 7 summarizes the dependence of lattice parameters on pressure extracted from the LeBail refinements. The evolution of the axial ratio c/a shows an anomaly around 15 GPa. Using the third-order Birch-Murnaghan equation of state (EOS), the pressure-volume curve was analyzed. The EOS parameters were extracted: the bulk modulus is found to be $B_0 = 60(1)$ GPa, the pressure derivative $B_0' = 4.51(9)$ GPa, and the zero-pressure volume $V_0 = 124.6(1)$ Å^3. The measured B_0 is much higher than the calculated value of 46.7 GPa from density function theory [25].

Combining the appearance of a double-peak feature in the PFY-XAS data as well as anomalous slope change in the axial ratio c/a above 15 GPa, an electronic structural transition associated with the d orbitals can be safely concluded. These rich results call for further theoretical calculations to provide insight into the detailed electronic changes under pressure.

IV. CONCLUSION

In this work, we have systematically investigated the magnetic ordering temperature, valence state, and structural evolution of $EuCd_2As_2$ under high pressure. External pressure drastically enhances the magnetic ordering temperature of the compound. The structural refinements show that the ambient trigonal structure of $EuCd_2As_2$ is maintained up to 34.6 GPa. Eu ions remain divalent up to 35.9 GPa. XRD and XAS data indicate an electronic transition around 15 GPa linked to

changes in detailed d-orbital populations. However, the previously predicted pressure-induced magnetic phase transition from AFM to FM with magnetic moments along the c axis is not evident in the present studies. Instead, the magnetic moments are found to orient primarily in the ab plane up to 42.8 GPa. The magnetic ordering temperature is significantly elevated under compression. These comprehensive experimental results will help improve future theoretical models in search of the desired Weyl state in this compound.

APPENDIX

To verify the magnetic ground state of the $EuCd_2As_2$ sample used in this study, the magnetization measurement was taken in the Quantum Design Physical Property Measurement System. Figure 8 shows that our $EuCd_2As_2$ sample grown from the Sn flux orders antiferromagnetically below 9.0 K. Fitting the data in the high-temperature region with Curie-Weiss law yields a magnetic moment of ~7.79(3) μ_B and Curie-Weiss temperature (θ) 8.82(2) K, in good agreement with the values reported in Ref. [19].

[1] X. Wan, A. M. Turner, A. Vishwanath, and S. Y. Savrasov, Phys. Rev. B **83**, 205101 (2011).

[2] A. A. Burkov, Nat. Mater. **15**, 1145 (2016).

[3] J. E. Moore, Nature (London) **464**, 194 (2010).

[4] M. Z. Hasan and C. L. Kane, Rev. Mod. Phys. **82**, 3045 (2010).

[5] Steven S.-L. Zhang, A. A. Burkov, I. Martin, and O. G. Heinonen, Phys. Rev. Lett. **123**, 187201 (2019).

[6] L. Šmejkal, T. Jungwirth, and J. Sinova, Phys. Status Solidi RRL **11**, 1700044 (2017).

[7] B. Yan and C. Felser, Annu. Rev. Condens. Matter Phys. **8**, 337 (2017).

[8] N. P. Armitage, E. J. Mele, and A. Vishwanath, Rev. Mod. Phys. **90**, 015001 (2018).

[9] S.-M. Huang, S.-Y. Xu, I. Belopolski, C.-C. Lee, G. Chang, B. Wang, N. Alidoust, G. Bian, M. Neupane, C. Zhang, S. Jia, A. Bansil, H. Lin, and M. Z. Hasan, Nat. Commun. **6**, 7373 (2015).

[10] A. A. Zyuzin and A. A. Burkov, Phys. Rev. B **86**, 115133 (2012).

[11] C.-X. Liu, P. Ye, and X.-L. Qi, Phys. Rev. B **87**, 235306 (2013).

[12] P. Hosur and X. Qi, C. R. Phys. **14**, 857 (2013).

[13] S. A. Parameswaran, T. Grover, D. A. Abanin, D. A. Pesin, and A. Vishwanath, Phys. Rev. X **4**, 031035 (2014).

[14] G. Hua, S. Nie, Z. Song, R. Yu, G. Xu, and K. Yao, Phys. Rev. B **98**, 201116(R) (2018).

[15] L.-L. Wang, N. H. Jo, B. Kuthanazhi, Y. Wu, R. J. McQueeney, A. Kaminski, and P. C. Canfield, Phys. Rev. B **99**, 245147 (2019).

[16] J.-R. Soh, F. de Juan, M. G. Vergniory, N. B. M. Schröter, M. C. Rahn, D. Y. Yan, J. Jiang, M. Bristow, P. Reiss, J. N. Blandy, Y. F. Guo, Y. G. Shi, T. K. Kim, A. McCollam, S. H. Simon, Y. Chen, A. I. Coldea, and A. T. Boothroyd, Phys. Rev. B **100**, 201102(R) (2019).

[17] Y. Xu, L. Das, J. Z. Ma, C. J. Yi, S. M. Nie, Y. G. Shi, A. Tiwari, S. S. Tsirkin, T. Neupert, M. Medarde, M. Shi, J. Chang, and T. Shang, Phys. Rev. Lett. **126**, 076602 (2021).

[18] M. C. Rahn, J.-R. Soh, S. Francoual, L. S. I. Veiga, J. Strempfer, J. Mardegan, D. Y. Yan, Y. F. Guo, Y. G. Shi, and A. T. Boothroyd, Phys. Rev. B **97**, 214422 (2018).

[19] N. H. Jo, B. Kuthanazhi, Y. Wu, E. Timmons, T.-H. Kim, L. Zhou, L.-L. Wang, B. G. Ueland, A. Palasyuk, D. H. Ryan, R. J. McQueeney, K. Lee, B. Schrunk, A. A. Burkov, R. Prozorov, S. L. Bud'ko, A. Kaminski, and P. C. Canfield, Phys. Rev. B **101**, 140402(R) (2020).

[20] J. Ma, H. Wang, S. Nie, C. Yi, Y. Xu, H. Li, J. Jandke, W. Wulfhekel, Y. Huang, D. West, P. Richard, A. Chikina, V. N. Strocov, J. Mesot, H. Weng, S. Zhang, Y. Shi, T. Qian, M. Shi, and H. Ding, Adv. Mater. **32**, 1907565 (2020).

[21] I. Schellenberg, U. Pfannenschmidt, M. Eul, C. Schwickert, and R. Pöttgen, Z. Anorg. Allg. Chem. **637**, 1863 (2011).

[22] H. P. Wang, D. S. Wu, Y. G. Shi, and N. L. Wang, Phys. Rev. B **94**, 045112 (2016).

[23] J.-Z. Ma, S. M. Nie, C. J. Yi, J. Jandke, T. Shang, M. Y. Yao, M. Naamneh, L. Q. Yan, Y. Sun, A. Chikina, V. N. Strocov, M. Medarde, M. Song, Y.-M. Xiong, G. Xu, W. Wulfhekel,

[24] J. Krishna, T. Nautiyal, and T. Maitra, Phys. Rev. B **98**, 125110 (2018).

[25] E. Gati, S. L. Bud'ko, L.-L. Wang, A. Valadkhani, R. Gupta, B. Kuthanazhi, L. Xiang, J. M. Wilde, A. Sapkota, Z. Guguchia, R. Khasanov, R. Valentí, and P. C. Canfield, Phys. Rev. B **104**, 155124 (2021).

[26] F. Du, L. Yang, Z. Nie, N. Wu, Y. Li, S. Luo, Y. Chen, D. Su, M. Smidman, Y. Shi et al., Quantum Mater. **7**, 65 (2022).

[27] Y. Wang, C. Li, T. Miao, S. Zhang, Y. Li, L. Zhou, M. Yang, C. Yin, Y. Cai, C. Song, H. Luo, H. Chen, H. Mao, L. Zhao, H. Deng, Y. Sun, C. Zhu, F. Zhang, F. Yang, Z. Wang et al., Phys. Rev. B **106**, 085134 (2022).

[28] W. Bi, J. Lim, G. Fabbris, J. Zhao, D. Haskel, E. E. Alp, M. Y. Hu, P. Chow, Y. Xiao, W. Xu, and J. S. Schilling, Phys. Rev. B **93**, 184424 (2016).

[29] S. Ikeda, Y. Tsuchiya, X.-W. Zhang, S. Kishimoto, T. Kikegawa, Y. Yoda, H. Nakamura, M. Machida, J. K. Glasbrenner, and H. Kobayashi, Phys. Rev. B **98**, 100502(R) (2018).

[30] W. Bi, Z. Nix, U. Dutta, J. Zhao, E. E. Alp, D. Zhang, P. Chow, Y. Xiao, Y.-B. Liu, G.-H. Cao, and Y. K. Vohra, Phys. Rev. B **103**, 195135 (2021).

[31] W. Bi, T. Culverhouse, Z. Nix, W. Xie, H.-J. Tien, T.-R. Chang, U. Dutta, J. Zhao, B. Lavina, E. E. Alp et al., npj Quantum Mater. **7**, 43 (2022).

[32] I. Sergueev, L. Dubrovinsky, M. Ekholm, O. Y. Vekilova, A. I. Chumakov, M. Zajac, V. Potapkin, I. Kantor, S. Bornemann, H. Ebert, S. I. Simak, I. A. Abrikosov, and R. Rüffer, Phys. Rev. Lett. **111**, 157601 (2013).

[33] J. Y. Zhao, W. Bi, S. Sinogeikin, M. Y. Hu, E. E. Alp, X. C. Wang, C. Q. Jin, and J. F. Lin, Rev. Sci. Instrum. **88**, 125109 (2017).

[34] A. Dewaele, M. Torrent, P. Loubeyre, and M. Mezouar, Phys. Rev. B **78**, 104102 (2008).

[35] W. Sturhahn, Hyperfine Interact. **125**, 149 (2000).

[36] W. Bi, N. M. Souza-Neto, D. Haskel, G. Fabbris, E. E. Alp, J. Zhao, R. G. Hennig, M. M. Abd-Elmeguid, Y. Meng, R. W. McCallum, K. Dennis, and J. S. Schilling, Phys. Rev. B **85**, 205134 (2012).

[37] Z. Nix, J. Zhao, E. E. Alp, Y. Xiao, D. Zhang, G.-H. Cao, Y. K. Vohra, and W. Bi, J. Phys.: Condens. Matter **34**, 415601 (2022).

[38] Y. Xiao, P. Chow, and G. Shen, High Press. Res. **36**, 315 (2016).

[39] B. Ravel and M. Newville, J. Synchrotron Radiat. **12**, 537 (2005).

[40] D. Zhang, P. K. Dera, P. J. Eng, J. E. Stubbs, J. S. Zhang, V. B. Prakapenka, and M. L. Rivers, J. Visual. Expt. **119**, e54660 (2017).

[41] C. Prescher and V. B. Prakapenka, High Press. Res. **35**, 223 (2015).

[42] B. H. Toby and R. B. Von Dreele, J. Appl. Crystallogr. **46**, 544 (2013).

[43] I. Nowik, B. D. Dunlap, and J. H. Wernick, Phys. Rev. B **8**, 238 (1973).

[44] Z. Yu, X. Chen, W. Xia, N. Wang, X. Lv, D. Wu, W. Wu, Z. Liu, J. Zhao, M. Li, S. Li, X. Li, Z. Dong, C. Zhou, L. Zhang,

X. Wang, N. Yu, Z. Zou, J. Luo, J. Cheng *et al.*, Adv. Quantum Technol. **6**, 2200128 (2023).

[45] G. M. Kalvius, G. K. Shenoy, G. J. Ehnholm, T. E. Katila, O. V. Lounasmaa, and P. Reivari, Phys. Rev. **187**, 1503 (1969).

[46] J. K. Desmarais, A. Erba, Y. Pan, B. Civalleri, and J. S. Tse, Phys. Rev. Lett. **126**, 196404 (2021).

[47] A. Salamat, R. Briggs, P. Bouvier, S. Petitgirard, A. Dewaele, M. E. Cutler, F. Corà, D. Daisenberger, G. Garbarino, and P. F. McMillan, Phys. Rev. B **88**, 104104 (2013).

[48] G. Deffrennes, P. Faure, F. Bottin, J.-M. Joubert, and B. Oudot, J. Alloys Compd. **919**, 165675 (2022).